Anthropogenic-induced changes in 21st Century summertime hydroclimatology of the Northeastern U.S.

BRUCE T. ANDERSON
Department of Geography and Environment, Boston University
Boston, MA 02215
brucea@bu.edu

KATHARINE HAYHOE
Dept. of Geosciences, Texas Tech University
Lubbock, TX 70409
katharine.hayhoe@ttu.edu

XIN-ZHONG LIANG
Illinois State Water Survey
Illinois Department of Natural Resources and
University of Illinois at Urbana-Champaign
xliang@uiuc.edu

Abstract Potential changes in summertime hydroclimatology over the northeastern (NE) region of the United States induced by increases in greenhouse gas (GHG) concentrations are investigated using a state-of-the-art regional climate modeling system. Results for a higher emissions scenario illustrate changes that may occur if dependence on fossil fuels continues over the coming century. Summertime precipitation is projected to decrease across much of the central NE, but increase over the southernmost and northernmost portions of the domain. Evaporation is expected to increase across the entire domain. The balance between these two results in a decrease in soil moisture content across most of the domain (by approximately 10mm) and an increase in the summertime soil-moisture depletion rate (by approximately 10mm/month). At the same time, an increase in both atmospheric near-surface specific and saturation specific humidity is projected, resulting in an increase in relative humidity across the southern portion of the domain, with slight decreases over the northern portion. Combined with an average increase in summer temperatures of 3.5°C, the projected increase in relative humidity results in a marked increase in the average daily maximum heat index for the region on the order of 3.9°C, as well as a 350-400% increase in the number of days with heat index values exceeding 32.2°C (90°F)—the level of "extreme caution". Taken together, these high-resolution, dynamically-generated projections confirm the potential for significant summertime climate change impacts on the NE over the coming century as suggested by previous studies.

1 Introduction

The Northeastern (NE) region of the United States is defined here to include Maine, New Hampshire, Vermont, Massachusetts, Rhode Island, Connecticut, New York, and the northeastern portion of Pennsylvania (Figure 1). Previous research has examined both historical climate variations and possible future climate change in this region, and has shown that this region is potentially susceptible to impacts on its natural and socio-economic systems (Hodgkins et al., 2002; Huntington, 2003; Huntington et al., 2004; Trombulak and Wolfson, 2004; Griffiths and Bradley, 2007; Hayhoe et al., 2007, 2008; Burakowski et al., 2008). Of particular importance are estimates of how the regional hydrologic cycle varies with global-scale climate change. Changes in the hydroclimatology—e.g. the long-term atmospheric and land surface processes that mediate the hydrologic cycle—can result in changes in mean and extreme rainfall, evaporation, soil-moisture content and soil-moisture recharge/discharge, streamflow, and human health. Related studies have identified existing and potential future impacts of climate change on regional ecology, including forests and agriculture (Iverson et al., 2008; Ollinger et al., 2008; Wolfe et al., 2008), and birds and pests (Subak, 2003; McCabe and Bunnell, 2004; Rodgers et al., 2007; Paradis et al., 2008; Rodenhouse et al., 2008); on land-surface hydrology, including drought, snow cover, and streamflow (Huntington, 2004; Hodgkins et al., 2005; Hayhoe et al., 2007; Marshall and Randhir, 2008); and on human health and welfare, including air quality, infrastructure, and the economy (Mickley et al., 2004; NECIA, 2006; Knowlton et al., 2007; Kirshen et al., 2008; Kunkel et al., 2008; Scott et al., 2008).

Many of the projected climate change impacts discussed above were based on simulations by global coupled atmosphere-ocean general circulation models (AOGCMs - Huntington, 2004;

Mickley et al., 2004; NECIA, 2006; Kirshen et al., 2008; Iverson et al., 2008), with grid-cells encompassing entire states (see Figure 1). However, previous studies have shown that regional topographic and geographic features—including the Appalachians to the south, the Catskills to the west, and the land-sea boundary to the east—influence the region's hydroclimatology (e.g. Magilligan and Graber, 1996) and variability (e.g. Bartlein, 1982; Leathers et al., 2000). In addition, multiple meso- and regional-scale dynamical processes also contribute to the climatology and variability of the region, including synoptic disturbances (Keim et al., 2005), tropical cyclone activity (Boose et al., 2001), land-sea breezes (Colby, 2004) and topographically-forced circulations (Wasula et al., 2002).

Given that many of these static and dynamic controls are unresolved by global model simulations, other studies of the climate change impacts on the NE have downscaled the global scale data to higher-resolution domains. In some cases, statistical downscaling approaches have been employed to alleviate the problems associated with coarse-scale global climate simulation output (Ollinger et al., 2008; Wolfe et al., 2008; Paradis et al., 2008; Rodenhouse et al., 2008; Scott et al., 2008; Marshall and Randhir, 2008). However these assume *a priori* statistical relationships between large-scale monthly temperature and precipitation maps and fine-scale daily time-series across the region (Vrac et al., 2007). Alternatively, other studies have employed dynamical downscaling techniques using numerically-based regional climate models (RCMs - Hodgkins et al., 2005; Knowlton et al., 2007; Kunkel et al., 2008). In this study we also use high resolution RCM data driven by AOGCM output fields to assess anthropogenically-induced variations in summertime land/atmosphere hydroclimatology for the region. A particular focus of the paper is on the geographic variations in precipitation, evaporation, soil moisture and humidity provided by these high-resolution regional climate forecasts. These estimates of how

the regional hydrologic cycle varies with global-scale climate change provide the foundation for assessing the sign and magnitude of a number of possible impacts on both human and natural systems across the NE. At the same time, these results should be considered plausible projections of climate change in this region, not necessarily forecasts of such change.

The outline of the paper is as follows: in Section 2 we present the data used in the study. Section 3 examines estimated changes in hydroclimatic parameters across the region; this section also examines the evolution of these changes over the course of the century to quantify the extent to which the climate impacts evolve linearly with heat-trapping gas concentrations (such as CO_2 and methane). Section 4 then presents the conclusions of this research.

2 Data and Models

This study is based on high-resolution regional climate model (RCM) simulations driven by output from historic and future simulations of the DOE/NCAR Parallel Climate Model (PCM - Washington et al., 2000). The historic simulation corresponds to the Coupled-Model Intercomparison Project "20th Century Climate in Coupled Models" scenario (20C3M, Covey et al., 2004), driven by historically-accurate forcings including anthropogenic emissions of greenhouse gases and aerosols, indirect effects on atmospheric water vapor and ozone, and natural changes in solar radiation and volcanic emissions.

The future simulation is forced by the A1fi emissions scenario from the IPCC Special Report on Emission Scenarios (SRES, Nakićenović et al., 2000). The A1fi scenario represents a higher emissions pathway over the coming century, assuming a continued reliance on fossil fuels albeit with relatively rapid technological development. For this scenario, atmospheric CO_2 concentrations reach approximately 567 parts per million by volume (ppm) by 2050 and 970

ppm by 2100. The PCM model is one of twenty-three AOGCMs that have submitted simulations to the IPCC Fourth Assessment Report (AR4). With a global climate sensitivity of 1.32^{o}C (Tebaldi et al., 2006), below the observationally-constrained "very likely" lowest estimate of climate sensitivity of 1.5^{o}C (Hegerl et al., 2007), the PCM is the least sensitive of the AR4 AOGCMs at the global scale. At the regional scale, PCM-driven projections for the Northeast are at the lower end of the range of AOGCM simulations, but are not the lowest (not shown). As such, the magnitude of future climate projections generated by the PCM—particularly for temperature-related changes—should be interpreted as representing a lower-boundary on what might be expected under the emissions scenario considered here.

Given the relatively coarse scale resolution of PCM simulations (T42 or approximately 300x300 km), we use a RCM to conduct dynamical downscaling integrations and provide improved mesoscale projections for assessing potential climate change impacts at the regional scale. For this study, we use the CMM5, the climate extension of the fifth-generation Pennsylvania State University-Nation Center for Atmospheric Prediction (PSU-NCAR) Mesoscale Model (MM5) version 3.3 (Dudhia et al., 2000) as developed by Liang et al. (2001, 2006). Important improvements include incorporation of more realistic surface boundary conditions and cloud cover prediction. Here the CMM5 is run at a 30-km grid spacing with output provided every 3 hours. It is forced at the regional lateral boundaries by the 6-hourly output from the 20C3M PCM simulations for the historical Spring/Summer period (April-August) from 1990-1999 and by future A1fi simulations for the future Spring/Summer periods 2045-2054 and 2090-2099; for this research we will only be examining the summertime (June-August) period, which removes the "spin-up" effects during the first 1-2 months associated with the sensitivity of the system to initial surface boundary conditions. As with the coarser-scale

PCM simulations, none of the results are calibrated against the period of overlapping observations (i.e. 1990-1999); instead the evolution of the hydroclimatic parameters in both model systems is dictated by the internal dynamic, thermodynamic and hydrologic evolution of the model system itself. Our analysis here focuses primarily on the differences between the 1990-1999 and 2090-2099 summertime periods, while the 2045-2054 period is checked for consistency and linearity.

3 Results

3.1 Comparison of AOGCM and RCM historical simulations to observations

The CMM5 has demonstrated a pronounced skill in downscaling regional-scale precipitation, soil moisture, and surface air temperature (Liang et al., 2004a, 2004b, 2006; Hayhoe et al., 2008) over the NE and the U.S. in general. Here we assess CMM5 downscaling skill over the NE in comparison to precipitation and temperature data taken from the Historical Climatology Network station observations (HCN - Karl et al, 1990) and historical AOGCM (PCM) simulations.

First, we compare the spatial distributions of observed and simulated mean summer (June-August) precipitation amounts across the NE (Figure 1). The relatively coarse-resolution PCM (with only 8 grid-points covering the NE) obscures many regional details, although the overall amounts are similar to observed values. In comparison, the higher-resolution RCM better captures the spatial distributions of mean precipitation amounts across the domain, including the enhanced precipitation amounts along the elevated regions of Vermont/New Hampshire and upstate New York. However, the overall amounts tend to be lower than observed, particularly

along the coastal regions in the NE's southern portion (see Figure 3), where lighter precipitation is likely due to the cumulus parameterization used in the model (Liang et al., 2004a).

Figure 2 compares the observed and simulated summer mean daily temperature maximums over the NE. The PCM values are significantly cooler than observed, while the RCM results are more realistic. In particular, the RCM captures many spatial details of the observed temperature distribution, with higher temperatures along the southern coast and lower values across the northern portions of New York, extending into the northern inland portions of New Hampshire, Vermont and Maine.

The differences between the simulated (PCM and RCM) precipitation and temperature fields, compared with the observed fields, are shown in Figure 3. Here, the simulated station measurements are selected by taking the grid-point value in which a given station is found and assigning that value to the simulated estimate. Differences are then taken between the simulated estimate and the observed value at the given station. Overall, the coarse-scale data from the PCM captures the seasonal rainfall totals over much of the region fairly well. In comparison, the fine-scale RCM data tend to underestimate precipitation over much of the domain, particularly along the coastal regions in the southern portion of the domain. As suggested above, this dry-bias in the RCM is most likely due to the cumulus parameterization within the RCM. Conversely, for estimates of daily maximum temperatures, the coarse-scale PCM has a cool bias over almost the entire domain; in contrast, the daily maximum temperatures in the RCM better capture the observed values, except along the coastal regions where precipitation is under-predicted.

It is important to note that while the coarse-scale PCM appears to better capture the seasonal totals in precipitation (although not the daily maximum temperatures), it may not

necessarily capture the distribution of daily precipitation events themselves. To determine how each model is representing the distribution of daily precipitation and maximum temperature values across the domain, we examine the probability distribution functions (PDFs) of summer (Jun-Aug) daily precipitation and daily maximum temperatures (Figure 4). For precipitation, we only consider days in which daily rainfall amount exceeds 2.5mm. Overall, we find that while the seasonal-total precipitation amounts from the PCM seem to match the observations (see Figure 1), the PCM simulations exhibit the typical "drizzle" problem of many AOGCMs, namely containing too many light-rainfall days, and not enough heavy-rainfall days as compared to observations for the period 1990-1999. In contrast, while the RCM slightly underestimates the number of rainfall days between 5–40 mm/day (leading to the overall dry-bias across the domain – see Figure 3), it has a significantly better overall frequency distribution when compared to the observed precipitation. For daily maximum temperature, the PCM produces large cold biases and an overly narrow distribution. On the other hand, the RCM-downscaled distribution is significantly closer to observed. In particular, the RCM captures both tails of the distribution, although it slightly overestimates the mean.

These comparisons, along with others (Liang et al., 2006; Hayhoe et al., 2008) suggest that the CMM5 is able to represent the mean spatial pattern, daily frequency distribution, and extreme value size and probability of the NE summer temperatures. Similarly, the RCM realistically captures the daily frequency distribution, magnitude, and probability of precipitation, as well as the mean spatial pattern across the region, although the model tends to under-predict overall seasonal rainfall amounts across the domain. Next, we examine CMM5 future simulations to determine how these climatic and other hydroclimatological parameters are projected to change under higher CO_2 concentrations associated with the A1fi scenario.

3.2 Future Changes in Seasonal Mean Fields

Projected future changes in mean seasonal summer precipitation and evaporation over the NE under the A1fi scenario, for 2090-2099 as compared to 1990-1999, are shown in Figure 5. Precipitation is projected to decrease along the northern coast and inland across Massachusetts, Vermont, New Hampshire, Maine and parts of upstate New York, but increase over the southern-most portions of the domain including Connecticut, Rhode Island and the southern portions of New York. Additional increases in precipitation are projected to occur along the Canadian border of northern New York and Maine. In contrast, surface evaporation is projected to increase across almost the entire NE, with largest increases in the western and northern portion of the domain. Small decreases are found where precipitation decreases are largest.

Changes in precipitation and evaporation have important implications for land-surface hydrology. Figure 6 shows the projected RCM-simulated changes in summertime seasonal-mean net surface moisture flux (calculated as precipitation minus evaporation), total soil moisture content, and soil moisture tendency. Generally, the moisture flux has a similar geographic structure to the precipitation field (Figure 5a). Because of the systematic increase in evaporation across the domain, moisture fluxes decrease over almost the entire domain except for Rhode Island/Connecticut where precipitation increases are greatest. The decrease in the moisture flux causes an overall reduction in total soil moisture, with only slight increases over the northern-most portions of the domain (Figure 6b); these increases are related to enhanced springtime precipitation amounts, which produce positive soil-moisture changes that carry over into summer (not shown). The soil moisture tendency over the course of the 3-month summertime period (Figure 6c)—defined as the difference between the total soil moisture content at the end of the 3-

month time-period and at the beginning—is projected to decrease over all of the NE. Since the region experiences a general drawdown (or discharge) of soil moisture during summer, the projected negative values indicate an *enhanced* drawdown in the future. These results for the region as a whole are in qualitative agreement with those derived using land-surface hydrology models driven by statistically-downscaled PCM A1fi output (Hayhoe et al., 2007).

The change in evaporation, representative of moisture fluxes from the surface (Figure 5b), impacts atmospheric hydrology. Figure 7 shows the percent changes in 2-meter (2m) specific humidity, q_{2m}, saturation specific humidity, q_{2m}^{sat}, and relative humidity, RH_{2m}, between the present (1990-1999) and future (2090-2099) under the A1fi scenario. The percentage change is calculated as the difference between the two periods divided by the present-day value. Note that the percentage change in relative humidity, $\%\Delta RH_{2m}$, is given by:

$$RH_{2m} = \frac{q_{2m}}{q_{2m}^{sat}} \Rightarrow \%\Delta RH_{2m} = \%\Delta q_{2m} - \%\Delta q_{2m}^{sat}$$

Hence, although the absolute changes in specific humidity tend to be smaller than changes in saturation specific humidity values across the whole domain (not shown), relative humidity may still increase as it is determined by the difference in relative rather than absolute changes. Here we calculate RH_{2m} at each 3-hour interval based upon the specific and saturation specific humidity values before calculating the seasonal-mean values; hence the percentage change in seasonal mean values shown in Figure 7c does not necessarily equal the difference between the percentage changes in seasonal mean values of q_{2m} and q_{2m}^{sat}.

In terms of relative magnitudes, under this simulation the NE is projected to see an increase in specific humidity (i.e. the amount of water vapor) on the order of 25%. In addition, the saturation specific humidity is also expected to increase; the increases are projected to be greatest over the central region, accompanying the largest temperature increases (see below).

Over the southern portion of the domain, the percentage increase in specific humidity is larger than that of saturation specific humidity, resulting in an *increase* in relative humidity stretching from the coast through most of New York. To the north—over Vermont, Maine, and New Hampshire—the saturation specific humidity increases more than the specific humidity, leading to slightly smaller values of relative humidity.

These changes in relative humidity, combined with the expected temperature increases, may cause a significant change in the summertime heat index—a measure of how hot it actually "feels" for air temperatures over 26.7 ^{o}C (80^{o}F). Figure 8 shows the change in the summer mean daily-maximum temperature and heat index based on 3-hourly samples. The heat index (*HI*) in ^{o}F is defined as in Stull (2000) with temperature *T* in ^{o}F and relative humidity *RH* in *%*. The *HI* is set to *T* unless *T* is above 80^{o}F and *RH* is higher than 40%. For comparison with actual or dry-bulb air temperature, *HI* is converted back to ^{o}C.

As indicated in Figure 8, under this simulation daily maximum temperatures are projected to increase by 3.5°C on average for the domain, with largest increases over southern Maine, Vermont and New Hampshire where changes in soil moisture are greatest. However, when accounting for the increased relative humidity, the daily-maximum heat index is projected to increase by 3.9°C, with the largest changes (greater than 4°C) found along the coastal regions of Massachusetts, New Hampshire and Maine.

3.3 Projected Changes in Excessive Precipitation and Temperature Events

While mean fields provide some indication of the overall change in the climatology of the region, the welfare of many natural and human systems are often sensitive to intense/excessive events as well (Easterling et al., 2000; Meehl et al., 2000; Greenough et al., 2001; Tebaldi et al.,

2006). For that reason, we also examine projected changes in the magnitude and frequency of intense events associated with changes in the summertime hydroclimatology of the NE.

To examine changes in excessive precipitation and temperature events, we first determine the 10% exceedence threshold value for daily precipitation/temperature at each grid-point during the 1990-1999 period. The exceedence threshold for precipitation is defined at each grid-point as the precipitation amount corresponding to the 90^{th}-percentile on the cumulative distribution function, calculated from those days with daily rainfall greater than 2.5mm; for temperature we calculate the exceedence threshold using all 92 days of the summertime period. We then calculate the increase in frequency of events exceeding the historical 10% exceedence threshold during 2090-2099 as projected under the A1fi scenario.

For precipitation (Figure 9a), the frequency of intense precipitation events increases by up to 100% in certain locations (predominantly over the southern coastal regions and northwestern regions along the Canadian border); at other locations however, the frequency of intense precipitation events decreases by up to 50% (predominantly over the northern coastal region). In general, during summer, approximately two-thirds of the domain experiences an increase in the number of intense rainfall events, although the average increase in the number of intense rainfall events across the domain is relatively small (16%). This result is in contrast to changes for the April-May period, during which intense precipitation occurrences increase by up to 50% over almost the entire domain, with increases of up to 100% along the southern coastal regions of Massachusetts, Rhode Island, and Connecticut (not shown).

Under the A1fi simulation, the frequency of days with maximum temperatures above the historical 90% threshold at each grid-point is expected to increase by over 250% (e.g. by a factor of 2.5) across the entire the domain (Figure 9b) and up to 350-400% for some parts of New

Hampshire, Vermont, and upstate New York; the area-average increase is 300%. For the daily maximum heat index (Figure 9c), the percentage change increase in number of excessive-heat events averages 375% across the domain, with some regions in the southern NE experiencing an increase of up to 400-450%.

Projected changes in temperature exeedences can be more directly related to potential public health impacts by examining the total number of days estimated to exceed the National Weather Service's "extreme caution" daily maximum heat index value of 32.2^{o}C (90^{o}F) (Figure 10). During the 1990s, only a few individual grid-points across the NE average more than 30 days per summer season at or above the NWS "extreme caution" levels; almost all grid points have fewer than 20 days. Under the higher A1fi scenario, by the 2090s on average more than 60 such days (out of 92) are projected to occur each year along the heavily-populated corridor of the southern coastal regions; in addition, along the coastal regions stretching into Maine "extreme caution" levels are expected to be reached on more than 50% of the days during summer. Also shown are those regions in which the seasonal *mean* daily-maximum heat index values are expected to be above 32.2^{o}C (90^{o}F). Again, these regions are concentrated along the southern coastal regions. Previous research using AOGCM-generated values of regional temperature changes, combined with land-surface hydrology model estimates of relative humidity, produce consistent results and indicate regions in southern portions of NE are expected to experience future summertime heat-index values similar to present-day values in South Carolina/Georgia (NECIA, 2006). These findings are also consistent with earlier analyses indicating the likelihood of increased heat-related risk to human health under scenarios of future climate change across the U.S. and the NE (Patz et al., 2005; Ebi et al., 2006; McMichael et al., 2006; Knowlton et al., 2007).

3.4 Time-evolution of Projected Future Climate Changes

Changes in NE summertime land-atmosphere hydroclimatology estimated above correspond to an end-of-century (2090s) CMM5 simulation driven by the low-sensitivity PCM model for the higher A1fi emissions scenario. To quantify the extent to which the evolution of climate parameters derived from the regional climate change predictions vary linearly with greenhouse gas concentrations, we briefly compare the changes projected by the 2090s with those projected to occur under the same A1fi scenario around midcentury, or 2045-2054. Here we are not attempting to compare implied changes for *different* emissions scenarios, which may be dependent upon both the timing and magnitude of emissions. Instead, we are trying to identify whether particular parameters show non-linear time evolutions for a particular emissions scenario. These non-linear evolutions can include increasing/decreasing sensitivity with time, as well as "turning" points in which initial responses differ in both sign and magnitude from longer-term responses.

We first compare projected seasonal-mean precipitation for mid-century (2045-2054) vs. end-of-century (2090-2099). Using a scatterplot, precipitation anomalies are compared by plotting each mid-century grid-point precipitation anomaly against its corresponding end-of-century value (Figure 11a). A best-fit linear trend is also shown, to indicate whether the overall sign of the changes are consistent across the region. Mid-century precipitation anomalies by grid-cell show some scatter when plotted against the corresponding end-of-century anomalies. However, the linear trend indicates that changes of the same sign are projected for most grid-cells for both mid- and end-of-century. This analysis also highlights some important temporal aspects of the projected changes, with precipitation anomalies for many of the positive-anomaly

grid-points (i.e. along the coastal regions of the domain and over the northern portions of Maine – Figure 5a) being of similar magnitude for both the 2045-54 and 2090-99 periods. In contrast, for the regions projected to experience large decreases in precipitation, these anomalies do not occur until later in the coming century (as evidenced by the discrepancy between the 2045-54 and 2090-99 values). When scaled by the relative changes in GHG concentrations, however, the 2090-99 negative anomalies are smaller than those suggested by a linear evolution of the 2045-54 anomalies, indicating that across the domain the initial trends in precipitation during the first part of the century are larger than during the latter part of the century (not shown).

Similar analyses for the maximum daily temperatures, seasonal-mean soil moisture content, and maximum daily heat indices are shown in Figure 11b-d. For seasonal-mean maximum daily temperatures, it is apparent that the changes in temperatures during the 2045-54 period are significantly lower than for the 2090-99 period (by about 2^{o}C). However, unlike precipitation, these differences appear to be linearly related to changing GHG concentrations—when scaled by the relative changes in GHG concentrations the 2045-54 anomalies lie almost directly on the 2090-99 anomalies (not shown).

For soil moisture content, as with precipitation, the grid-point changes tend to be more scattered. Furthermore, the presence of many grid-points in the upper left-hand quadrant of the figure indicates that many locations projected to have higher-than-normal soil moisture by mid-century are actually projected to have lower-than-normal soil moisture by end-of-century. In other words, initial climate change appears to result in higher available soil moisture; these enhanced soil moisture values are driven predominantly by increased precipitation during the preceding April-May period (not shown). However as temperatures, and hence evaporation, continue to increase, these initial changes are reversed and soil moisture is projected to decrease.

As with the 2090-99 projections, these results are in qualitative agreement with previous research using land-surface hydrology models driven by statistically-downscaled PCM A1fi output, which project increases in soil moisture for the region as a whole during mid-century, followed by subsequent decreases by the end of the integration period (Hayhoe et al., 2007). For those few regions where the soil moisture content is projected to increase by end-of-century, anomalies are fairly similar to the mid-century changes, most likely because the soil has become saturated even under a smaller degree of climate change, indicating that additional excess precipitation could lead to heavier run-off and greater flooding.

With regard to increases in daily-maximum heat index values (Figure 11d), it appears that the most significant increases are projected to occur in the latter half of the century. Across most of the region, the daily maximum heat index increases by 1°C-1.5°C by mid-century. By the end of the century, these values on average have more than tripled to 3.9°C, with some regions experiencing increases of over 4°C. Similar to the temperature field, however, the heat index values during 2045-54 and 2090-99 are quasi-linearly related to greenhouse gas concentrations. When scaled by the relative changes in GHG concentrations the 2045-54 anomalies again lie very close to the 2090-99 anomalies (not shown).

4 Conclusions

Climate change over the coming century is projected to bring significant changes to the basic climatology and variability of the summertime land-atmosphere hydrologic cycle over the northeastern United States. While increased concentrations of radiatively-active species—predominantly greenhouse gases such as CO_2 and methane—have a global-scale impact on climate, it is the manifestation of these global-scale changes at regional scales that will determine

how the climate changes will impact both human and natural systems in the region. Using an RCM driven by low-sensitivity AOGCM simulations for the SRES A1fi (higher) emissions scenario, we estimate projected mid- and end-of-century changes in key temperature, precipitation, and hydrological climate indices. While other important climate and environmental parameters that would also be expected to impact the NE—such as changes in sea level, mid-latitude storm activity, air or water quality—were not considered here, the land-atmosphere hydrologic cycle has a direct and indirect impact upon many of these fields and hence serves as a starting point to investigate regional climate change and associated impacts.

Seasonal-mean summertime precipitation is expected to decrease over much of the region, particularly along the northern coastal regions extending into the mountainous regions of Vermont and New Hampshire. Increases are projected along the southern coastal region and the northern inland regions of New York and northern Maine. Because of the general increase in summertime temperatures across the domain, the summer evaporation rate is also expected to increase. The balance between the seasonal-mean precipitation and evaporation results in a decrease in net moisture flux to the land surface across most of the domain, with the exception of the southern portion of the domain (Rhode Island and Connecticut). In turn, the seasonal-mean soil moisture content across the domain also tends to decrease, while the soil-moisture drawdown (which is a typical feature of the summertime hydrologic balance in this region) appears to intensify.

Increased cycling of moisture from the land to atmosphere (via evaporation) is projected to increase the specific humidity by 25% by end-of-century. At the same time, increased temperatures also raise the saturation specific humidity. However, it appears that the changes in the two are not equivalent and that the relative humidity in the southern portion of the region will

increase by up to 5% by the 2090s relative to its 1990s value, while values in the northern portion are expected to decrease somewhat. This increase in relative humidity, coupled with the increase in temperatures themselves, translates into a significant increase in the daily maximum summer heat index for the region, averaging 3.9°C by end-of-century under the simulation examined here. In addition the number of days with daily maximum heat index values greater than the 1990s 90th percentile exceedence threshold are expected to increase by 350-450%. For many coastal regions, the daily maximum heat index is expected to rise above 32.2^{o}C (90^{o}F)—the NWS-defined "extreme caution" level—during more than 50% of summer days and may become the climatological norm for the southeastern portions of the region.

Similar changes but of lesser magnitude are projected by mid-century for most variables, with some notable exceptions. Generally, trends in daily maximum temperatures and daily-maximum heat index values appear to follow a quasi-linear evolution with increasing greenhouse gas concentrations. In contrast, positive seasonal-mean precipitation anomalies during the middle of the simulation period (2045-54) are of the same magnitude as those found at the end of the simulation (2090-99); negative seasonal-mean precipitation anomalies trends during the beginning of the simulation are also larger than those found near the end. For soil moisture, the time-evolution for many regions mirrors that of precipitation; in addition, a large fraction of grid-cells show increased values by mid-century followed by overall decreases by end-of-century.

Here, climate changes are estimated based on a higher emissions scenario but a low-sensitivity climate model; hence, the magnitude of projected changes estimated here are likely to lie close to the middle of the range of what would be expected based on the full set of SRES emission scenarios and IPCC AR4 AOGCM simulations for this region. Overall, these results suggest a fairly dramatic change in the NE's summertime land/atmospheric hydroclimatology

over the coming century. In addition, these results suggest that many significant impacts—including those influencing human health and water availability—are expected to be felt later in the century. Finally, the estimated direction of changes in most variables are consistent with those estimated by previous studies that used alternative methods to generate high-resolution regional climate projections. This has important implications for regional climate assessments, as extensive RCM simulations of future conditions are not yet generally available.

Acknowledgements: Dr. Anderson's research was supported by a Visiting Scientist appointment to the Grantham Institute for Climate Change, administered by Imperial College of Science, Technology, and Medicine. Dr. Liang's research has been funded in part by the United States Environmental Protection Agency Science to Achieve Results Award RD-318 83096301-0. We also acknowledge NOAA/ESRL/GSD and NCSA/UIUC for the supercomputing support. Thanks are also extended to the reviewers, as well as to numerous other readers, for all their insightful and constructive comments.

References

Bartlein PJ (1982) Streamflow anomaly patterns in the USA and southern Canada – 1951-1970. J Hydrology 57: 49-63

Boose E, Chamberlin K, Foster D (2001) Landscape and region impacts of hurricanes in New England. Ecological Mono 71: 27-48

Burakowski EA, et al (2008) Trends in wintertime climate in northeastern United States: 1965-2005. J. Geophys Res 113: DOI 10.1029/2008JD009870

Colby F (2004) Simulation of the New England sea breeze: The effect of grid spacing. Weather and Forecasting 19: 277-285.

Covey C, et al (2003) An overview of results from the coupled model intercomparison project (CMIP). Global and Planetary Change, 37:103-133

Dudhia JD, et al (2000) PSU/NCAR Mesoscale modeling system tutorial class notes and users guide: MM5 modeling system version 3

Easterling D, et al (2000) Climate extremes: Observations, modeling, and impacts Science, 289:2068-2074.

Ebi K, Mills D, Smith J, Grambsch A (2006) Climate change and human health impacts in the United States: An update on the results of the US National Assessment Env Health Perspectives 114:1318-1324

Greenough G, McGeehin M, Bernard S, Trtanj J, Riad J, Engelberg D (2001) The potential impacts of climate variability and change on health impacts of extreme weather events in the United States. Env Health Perspectives 109:191-198 Suppl 2

Griffiths M, Bradley R (2007) Variations of twentieth-century temperature and precipitation extreme indicators in the northeast United States. J Climate 20:5401-5417

Hayhoe K et al (2007) Past and future changes in climate and hydrological indicators in the U.S. Northeast. Clim Dyn DOI 10.1007/s00382-006-0187-8

Hayhoe K et al (2008) Regional Climate Change Projections for the Northeast USA. Mitigation and Adaptation Strategies for Global Change DOI 10.1007/s11027-007-9133-2

Hegerl GC et al (2007) Understanding and Attributing Climate Change In: Climate Change (2007): The Physical Science Basis Contribution of Working Group I to the Fourth Assessment Report of the Intergovernmental Panel on Climate Change [Solomon, S, D Qin, M Manning, Z Chen, M Marquis, KB Averyt, M Tignor HL Miller (eds)] Cambridge University Press, Cambridge, United Kingdom and New York, NY, USA

Hodgkins GA, James I, Huntington T (2002) Historical changes in lake ice-out dates as indicators of climate change in New England, 1850-2000. Int J Climatology 22:1819-1827,

Hodgkins GA, Dudley RW, Huntington TG (2005) Summer low flows in New England during the 20th century. J Amer Water Resources Assoc 41:403-412

Huntington T, Hodgkins G, Keim B, Dudley R (2004) Changes in the proportion of precipitation occurring as snow in New England (1949-2000). J Climate 17:2626-2636

Huntington T (2003) Climate warming could reduce runoff significantly in New England, USA. Ag & Forest Met 117:193-201

Iverson L, Prasad A, Matthews S (2008) Modeling potential climate change impacts on the trees of the northeastern United States. Mitigation & Adaptation Strategies for Global Change DOI 10.1007/s11027-007-9129-y

Karl TR, Williams Jr CN, Quinlan FT, Boden TA (1990) United States Historical Climatology Network (HCN) Serial Temperature and Precipitation Data. Environmental Science Division, Publication No.3404, Carbon Dioxide Information and Analysis Center, Oak Ridge

National Laboratory, Oak Ridge, TN, 389pp

Keim B, Meeker L, Slater J (2005) Manual synoptic climate classification for the East Coast of New England (USA) with application to PM2.5 concentration. Climate Res 28: 143-154

Kirshen P, Watson C, Douglas E, Gontz A, Lee J, Tian Y (2008) Coastal flooding in the Northeastern United States due to climate change. Mitigation & Adaptation Strategies for Global Change DOI 10.1007/s11027-007-9130-5

Knowlton K et al (2007) Projecting heat-related mortality impacts under a changing climate in the New York City region. Am J Public Health 97:2028-2034

Kunkel K et al (2008) Sensitivity of future ozone concentrations in the northeast USA to regional climate change. Mitigation and Adaptation Strategies for Global Change DOI 10.1007/s11027-007-9137-y

Leathers DJ, Grundstein AJ, Ellis AW (2000) Growing season moisture deficits across the northeastern United States. Climate Res 14: 43-55

Liang X-Z, Pan JP, Zhu JH, Kunkel KE, Wang JXL, Dai AG (2006) Regional climate model downscaling of the U.S. summer climate and future change. J Geophys Res 111:Art. No. D10108

Liang X-Z, Kunkel KE, Samel AN (2001) Development of a regional climate model for US. Midwest applications. Part I: Sensitivity to buffer zone treatment. J Climate 14:4363–4378

Liang X-Z, Li L, Dai A, Kunkel KE (2004a) Regional climate model simulation of summer precipitation diurnal cycle over the United States. Geophys Res Lett 31:L24208 10.1029/2004GL021054

Liang X-Z, Li L, Kunkel KE, Ting MF, Wang JXL (2004b) Regional climate model simulation of U.S. precipitation during 1982–2002. Part 1: Annual cycle. J Climate 17:3510–3528

Magilligan FJ, Graber BE (1996) Hydroclimatological and geomorphic controls on the timing and spatial variability of floods in New England, USA. J Hydro 1788: 159-180

Marshall E, Randhir T (2008) Effect of climate change on watershed system: a regional analysis. Climatic Change 89: 263-280

McCabe GJ, Bunnell JE (2004) Precipitation and the occurrence of Lyme disease in the northeastern United States. Vector-Bourne and Zoonotic Diseases 4:143-148

McMichael A, Woodruff R, Hales S (2005) Climate change and human health: present and future risks. Lancet 367:859-869

Meehl G et al (2000) An introduction to trends in extreme weather and climate events: Observations, socioeconomic impacts, terrestrial ecological impacts, and model projections. Bull Am Met Soc 81:413-416

Mickley L, Jacob D, Field B, Rind D (2004) Effects of future climate change on regional air pollution episodes in the United States. Geophys Res Lett 31:L24103

Nakićenović N et al (2000) Special report on emissions scenarios: A special report of Working Group III on the Intergovernmental Panel on Climate Change. Cambridge University Press Cambridge, UK and New York, NY

NECIA (The Northeast Climate Impacts Assessment), 2006: Climate Change in the U.S. Northeast: A Report of the Northeast Climate Impacts Assessment. UCS Publications Cambridge, MA

Ollinger S, Goodale CL, Hayhoe K, Jenkins JP (2008) Potential effects of climate change and rising CO_2 on ecosystem processes in northeastern U.S. forests. Mitigation and Adaptation Strategies for Global Change DOI 10.1007/s11027-007-9128-z

Paradis A, Elkinton J, Hayhoe K, Buonaccorsi J (2008) Role of winter temperature and climate change on the survival and future range expansion of the hemlock woolly adelgid (Adelges tsugae) in eastern North America. Mitigation and Adaptation Strategies for Global Change DOI 10.1007/s11027-007-9127-0

Patz J, Campbell-Lendrum D, Holloway T, Foley J (2005) Impact of regional climate change on human health. Nature 438:310-317

Rodenhouse N et al (2008) Potential effects of climate change on birds of the Northeast. Mitigation & Adaptation Strategies for Global Change DOI 10.1007/s11027-007-9126-1

Rodgers SE, Zolnik CP, Mather TN (2007) Duration of exposure to suboptimal atmospheric moisture affects nymphal blacklegged tick survival. J Medical Entomology 44:372-375

Scott D, Dawson J, Jones B (2008) Climate change vulnerability of the US Northeast winter recreation– tourism sector. Mitigation & Adaptation Strategies for Global Change DOI 10.1007/s11027-007-9136-z

Subak K (2003) Effects of climate on variability in Lyme disease incidence in the northeastern United States. Amer J Epidemiology 157:531-538

Stull RB (2000) Meteorology for Scientists Engineers, 2nd Edition, Brooks Cole, 490 pp

Tebaldi C, Hayhoe K, Arblaster J, Meehl G (2006) Going to the extremes. Climatic Change 79:185-211

Trombulak S, Wolfson R (2004) Twentieth-century climate change in New England and New York, USA. Geophys Res Lett 31:L19202

Vrac M, Stein M, Hayhoe K, Liang X-Y (2007) A general method for validating statistical downscaling methods under future climate change. Geophys Res Lett 34:doi:10.1029/2007GL030295

Washington WM et al (2000) Parallel Climate Model (PCM) control and transient simulations. Clim Dynamics 16:755-774

Wasula AC, Bosart LF, LaPenta KD (2002) The influence of terrain on the severe weather distribution across interior Eastern New York and Western New England. Weather and Forecasting 17: 1277-1289.

Wolfe DW, Ziska L, Petzoldt C, Seaman A, Chase L, Hayhoe K (2008) Projected change in climate thresholds in the Northeastern U.S.: implications for crops, pests, livestock, and farmers. Mitigation and Adaptation Strategies for Global Change DOI 10.1007/s11027-007-9125.

FIGURE CAPTIONS

FIG.1 Mean 1990-1999 summertime (June-August) precipitation (mm/season) from (a) station observations (HCN), (b) global climate model 20C3M simulation (PCM), and (c) PCM-driven regional climate model simulation (RCM). For the station-based observations, the radius of the circle at each station is proportional to precipitation amount; actual amounts are given by the scale on the right-hand side.

FIG.2 Mean 1990-1999 summertime daily maximum temperatures (ºC) taken from (a) station observations (HCN), (b) global climate model 20C3M historical simulation (PCM), and (c) PCM-driven regional climate model simulation (RCM). For the station-based observations the radius of circle at each station is proportional to daily maximum temperature values; actual values are given by the scale on the right-hand side.

FIG.3 Difference in the mean 1990-1999 summertime (June-August) precipitation (mm/season) between (a) the global climate model 20C3M simulation (PCM) and station observations (HCN); and (b) the PCM-driven regional climate model simulation (RCM) and station observations (HCN). The radius of the circle at each station is proportional to the difference in precipitation amount; actual amounts are given by the scale on the right-hand side. (c,d) same as (a,b) except for the difference in the mean 1990-1999 summertime (June-August) daily maximum temperatures (ºC).

FIG.4 (a) Distribution of 1990-1999 grid-point daily summertime (a) precipitation (mm/day) and (b) maximum temperature (ºC) values over the NE from station observations (HCN), global climate model (PCM), and regional climate model (RCM). Here events represent the number of days which experience a given precipitation rate (maximum temperature). For (a), only days with precipitation amounts greater than 5mm/day are included, while for (b), all 92 days per season are considered.

FIG.5 Difference in RCM-simulated summertime seasonal-mean (a) precipitation and (b) evaporation from 1990-1999 to 2090-2099 as simulated under the A1fi emissions scenario. In both plots negative values represent a net loss of moisture from the underlying surface (e.g. a decrease in precipitation or an increase in evaporation) Units are in mm/season for both figures.

FIG.6 Difference in RCM-simulated summertime seasonal-mean (a) net moisture flux (mm/season, calculated as precipitation minus evaporation), (b) total moisture content (mm - note change in scale), and (c) total soil moisture tendency over 3-month period (mm/season) between 2090-2099 and 1990-1999 under the A1fi scenario.

FIG.7 Percent change in RCM-simulated summertime seasonal-mean (a) specific humidity, (b) saturation specific humidity, and (c) relative humidity in 2090-2099 relative to 1990-1999 under the A1fi scenario. Note change in scale in (c).

FIG.8 Difference in RCM-simulated summertime seasonal-mean daily maximum (a) 2-meter air temperatures (ºC) and (b) Heat Index (HI - ºC) between 2090-99 and 1990-99 under the A1fi scenario.

FIG.9 Percent change in number of days during 2090-99 experiencing daily (a) precipitation amounts, (b) maximum 2-meter air temperatures and (c) maximum Heat Index (HI) values greater than the 1990-99 10% exceedence threshold under the A1fi scenario.

FIG.10 Number of days per 92-day summer season (June-August) in which the daily heat index (HI) maximum is above the National Weather Service "extreme caution" level (90°F) for (a) 1990-1999 and (b) 2090-2099. Regions with black dots are ones in which seasonal-mean daily HI maximum is above "extreme caution" level (90°F).

FIG.11 Scatter plot of grid-point change in mean summertime precipitation (mm/season) between 1990-99 period and 2090-99 and 2045-54 periods, respectively, under the A1fi scenario. (blue) – 2090-99 precipitation anomalies plotted against themselves; (red) – 2045-54 precipitation anomalies plotted against the 2090-99 anomalies; (red line) – best-fit linear trend to the 2045-54 precipitation anomalies as plotted against the 2090-99 anomalies – see text for details. (b) same as (a) except for change in seasonal mean daily maximum temperatures (ºC). (c) same as (a) except for change in seasonal mean total soil moisture content (mm). (d) same as (a) except for change in seasonal mean daily maximum heat index (°C).

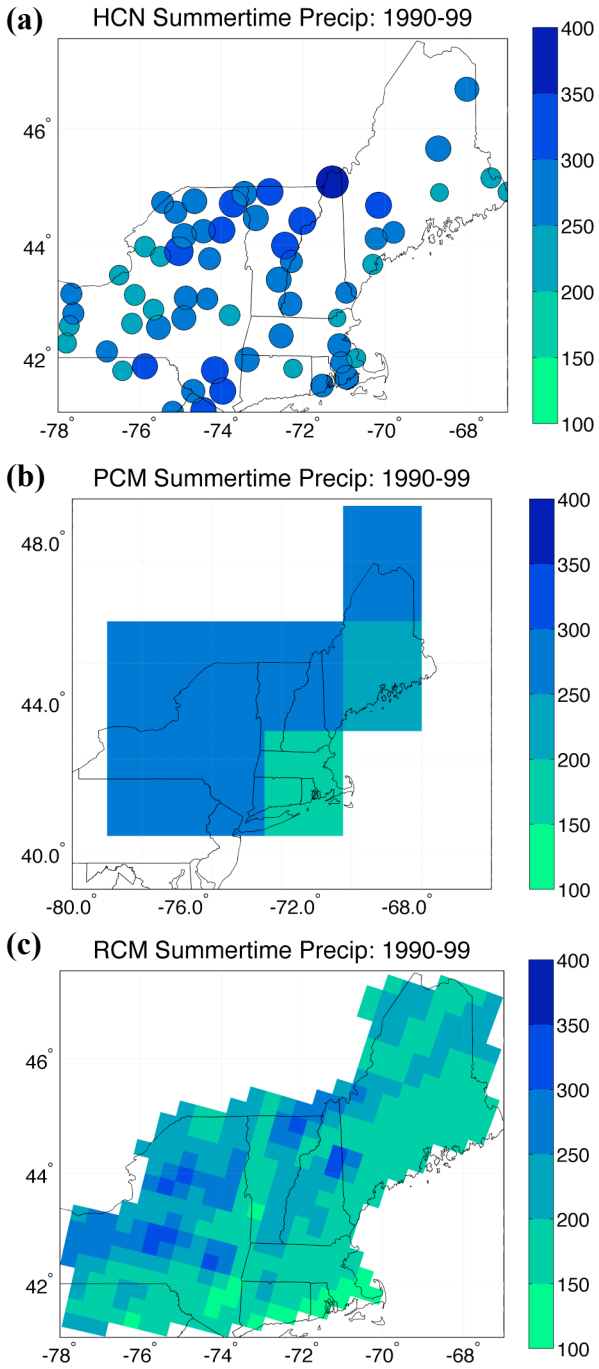

FIG.1 Mean 1990-1999 summertime (June-August) precipitation (mm/season) from (a) station observations (HCN), (b) global climate model 20C3M simulation (PCM), and (c) PCM-driven regional climate model simulation (RCM). For the station-based observations, the radius of the circle at each station is proportional to precipitation amount; actual amounts are given by the scale on the right-hand side.

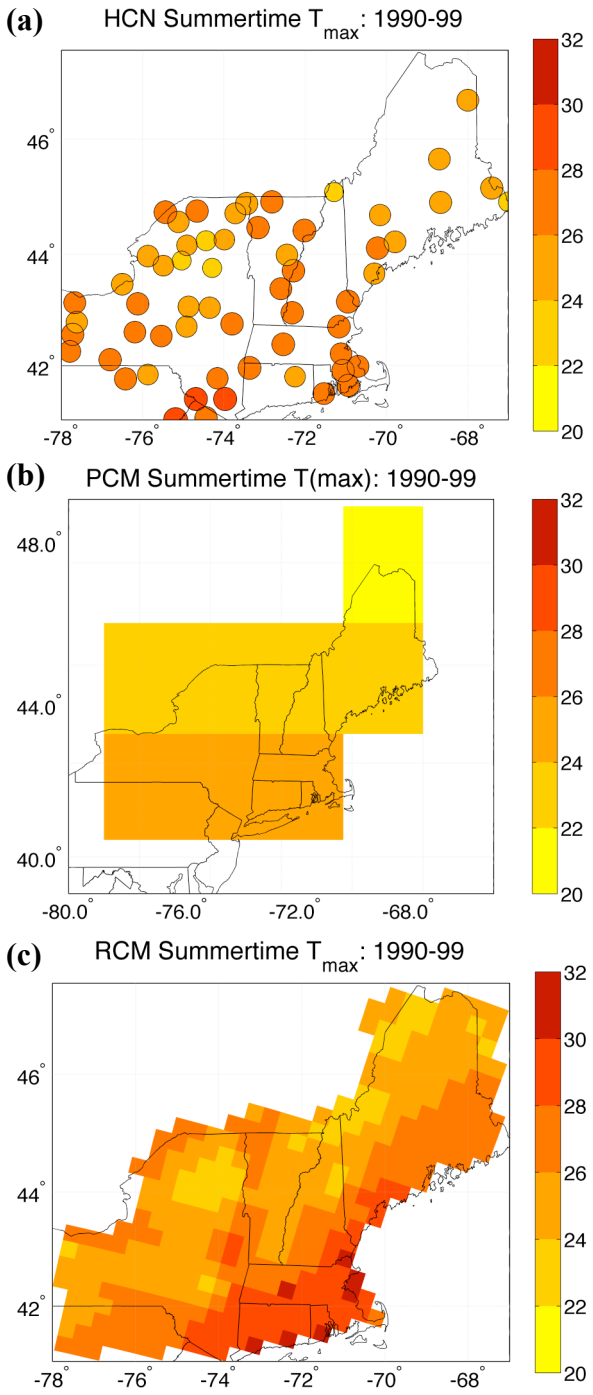

FIG.2 Mean 1990-1999 summertime daily maximum temperatures (°C) taken from (a) station observations (HCN), (b) global climate model 20C3M historical simulation (PCM), and (c) PCM-driven regional climate model simulation (RCM). For the station-based observations the radius of circle at each station is proportional to daily maximum temperature values; actual values are given by the scale on the right-hand side.

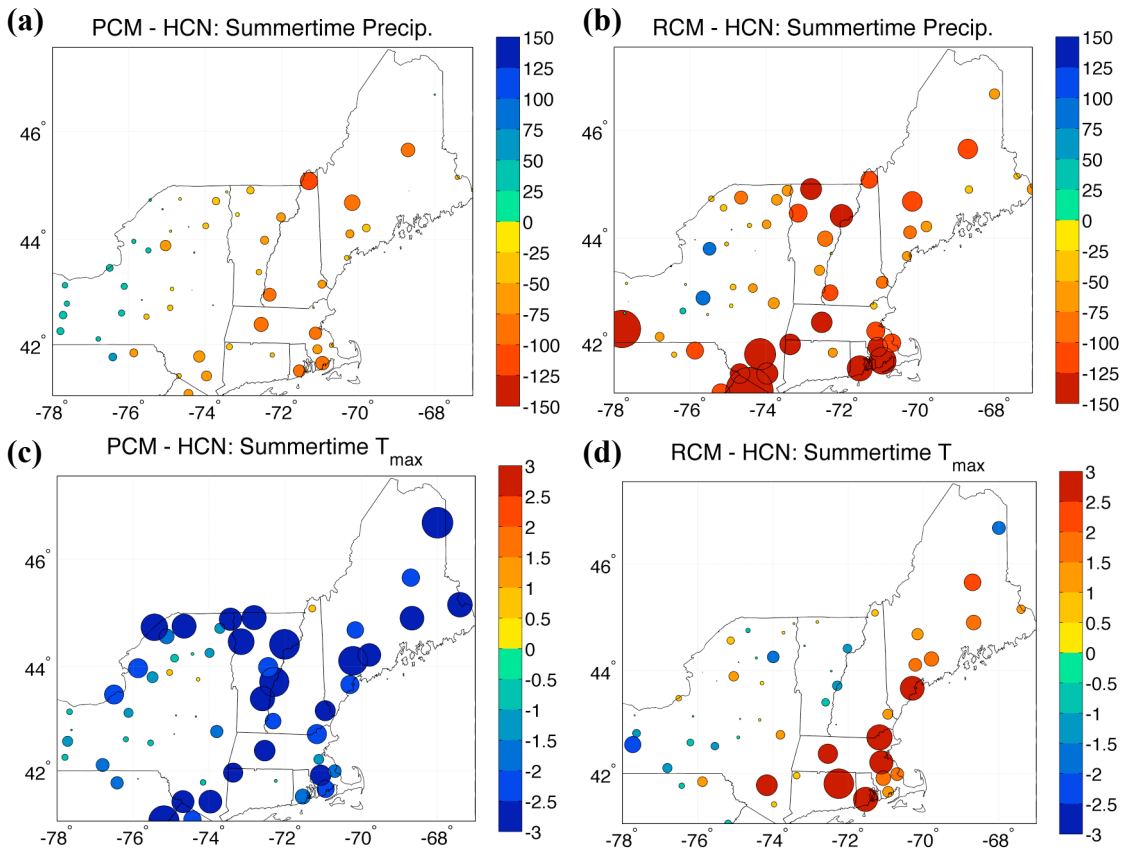

FIG.3 Difference in the mean 1990-1999 summertime (June-August) precipitation (mm/season) between (a) the global climate model 20C3M simulation (PCM) and station observations (HCN); and (b) the PCM-driven regional climate model simulation (RCM) and station observations (HCN). The radius of the circle at each station is proportional to the difference in precipitation amount; actual amounts are given by the scale on the right-hand side. (c,d) same as (a,b) except for the difference in the mean 1990-1999 summertime (June-August) daily maximum temperatures (^{o}C).

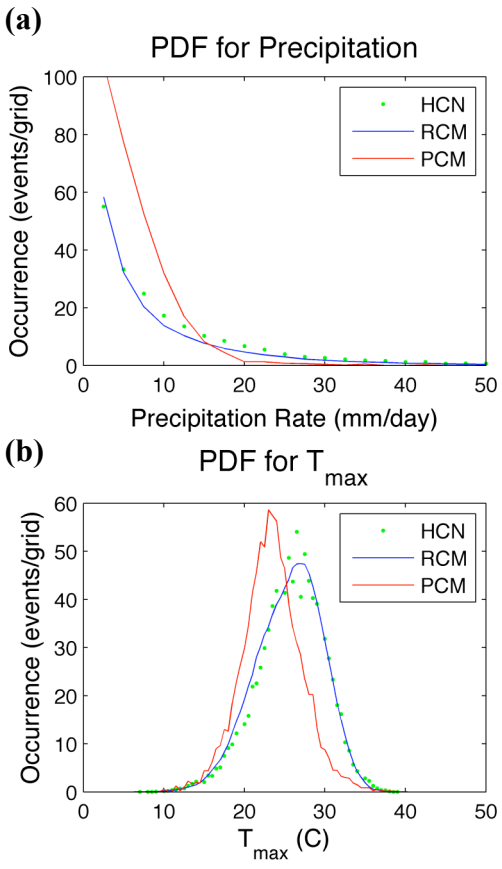

FIG.4 (a) Distribution of 1990-1999 grid-point daily summertime (a) precipitation (mm/day) and (b) maximum temperature (^{o}C) values over the NE from station observations (HCN), global climate model (PCM), and regional climate model (RCM). Here events represent the number of days which experience a given precipitation rate (maximum temperature). For (a), only days with precipitation amounts greater than 5mm/day are included, while for (b), all 92 days per season are considered.

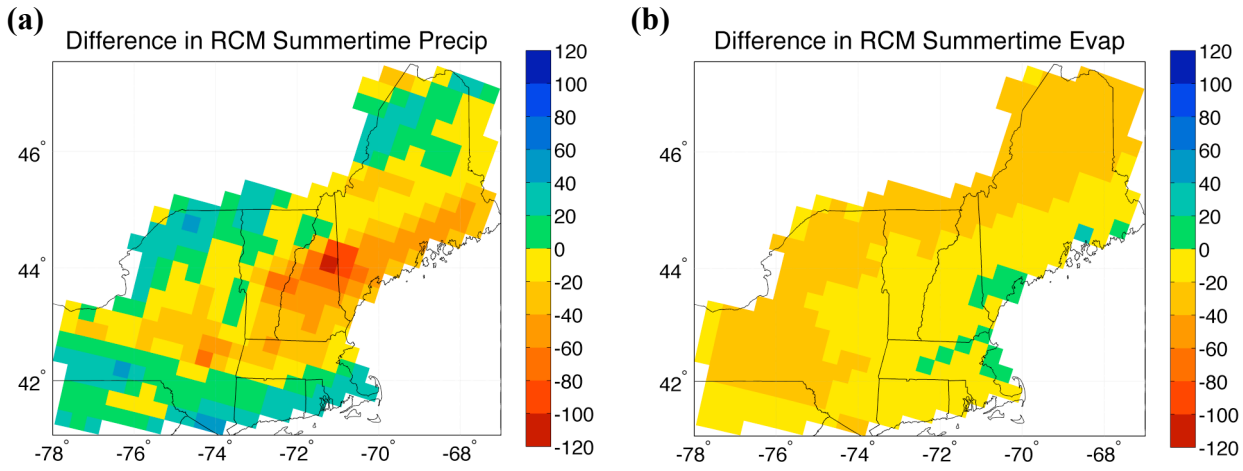

FIG.5 Difference in RCM-simulated summertime seasonal-mean (a) precipitation and (b) evaporation from 1990-1999 to 2090-2099 as simulated under the A1fi emissions scenario. In both plots negative values represent a net loss of moisture from the underlying surface (e.g. a decrease in precipitation or an increase in evaporation) Units are in mm/season for both figures

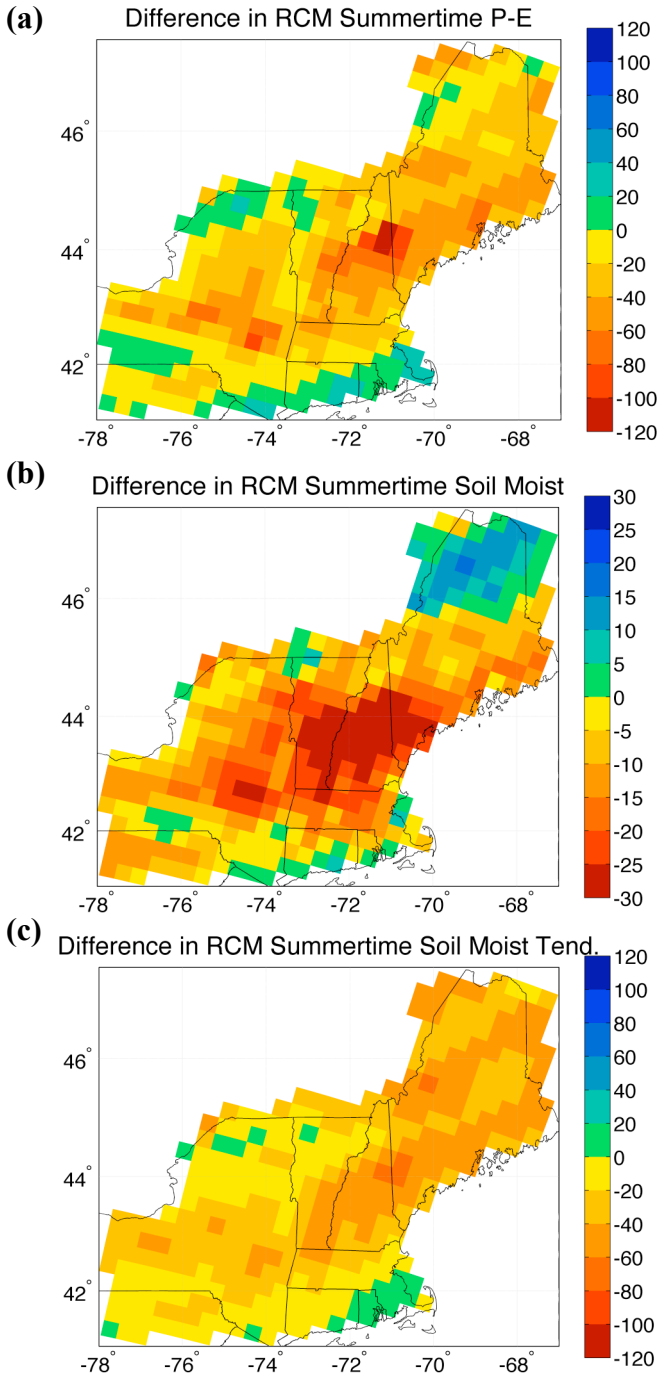

FIG.6 Difference in RCM-simulated summertime seasonal-mean (a) net moisture flux (mm/season, calculated as precipitation minus evaporation), (b) total moisture content (mm - note change in scale), and (c) total soil moisture tendency over 3-month period (mm/season) between 2090-2099 and 1990-1999 under the A1fi scenario.

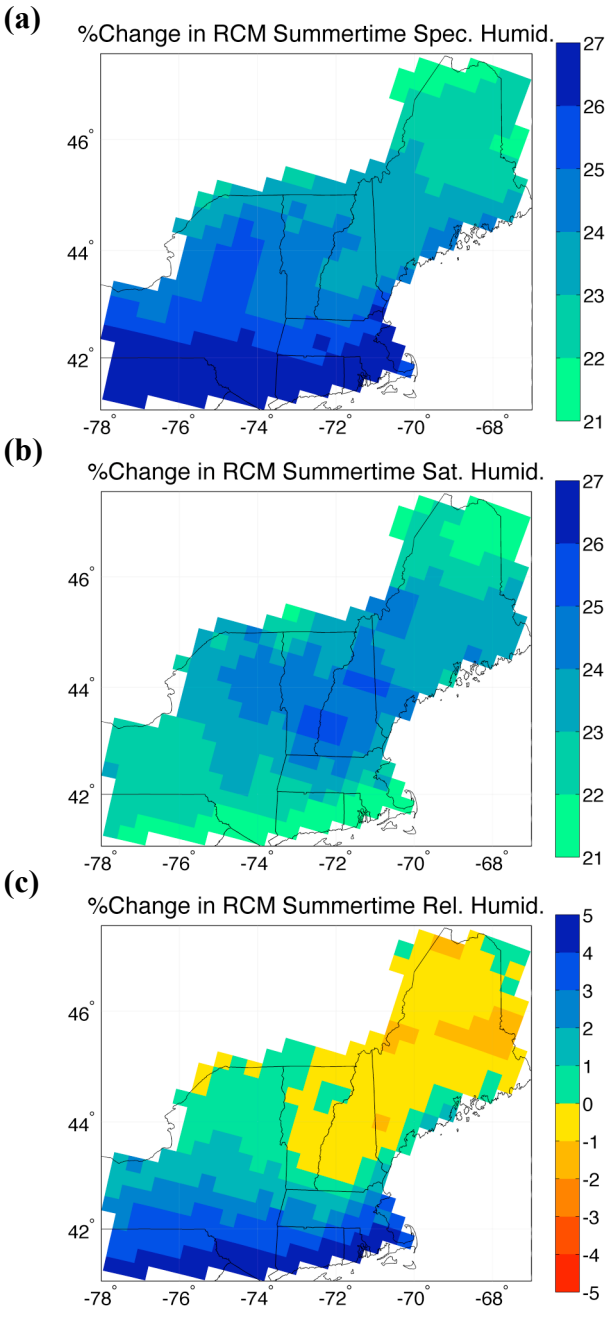

FIG.7 Percent change in RCM-simulated summertime seasonal-mean (a) specific humidity, (b) saturation specific humidity, and (c) relative humidity in 2090-2099 relative to 1990-1999 under the A1fi scenario. Note change in scale in (c).

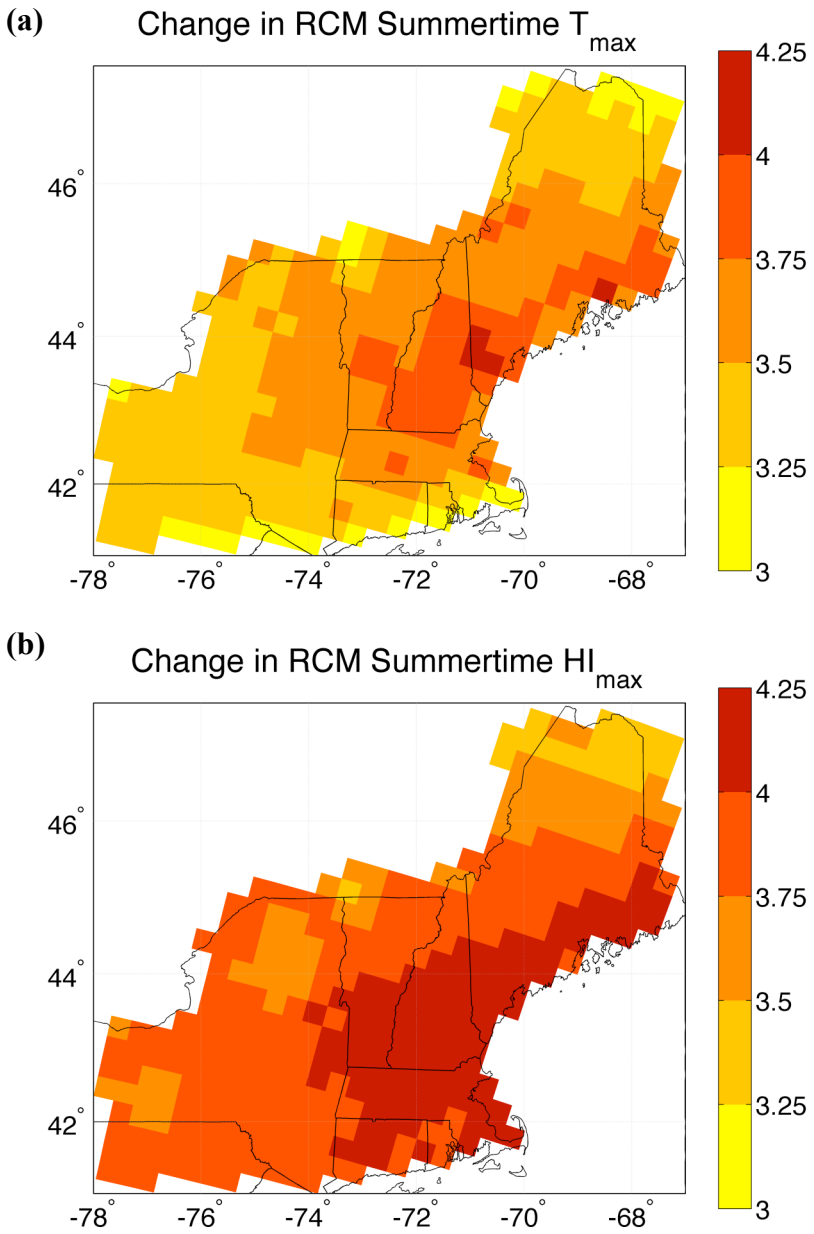

FIG.8 Difference in RCM-simulated summertime seasonal-mean daily maximum (a) 2-meter air temperatures (^{o}C) and (b) Heat Index (HI - ^{o}C) between 2090-99 and 1990-99 under the A1fi scenario.

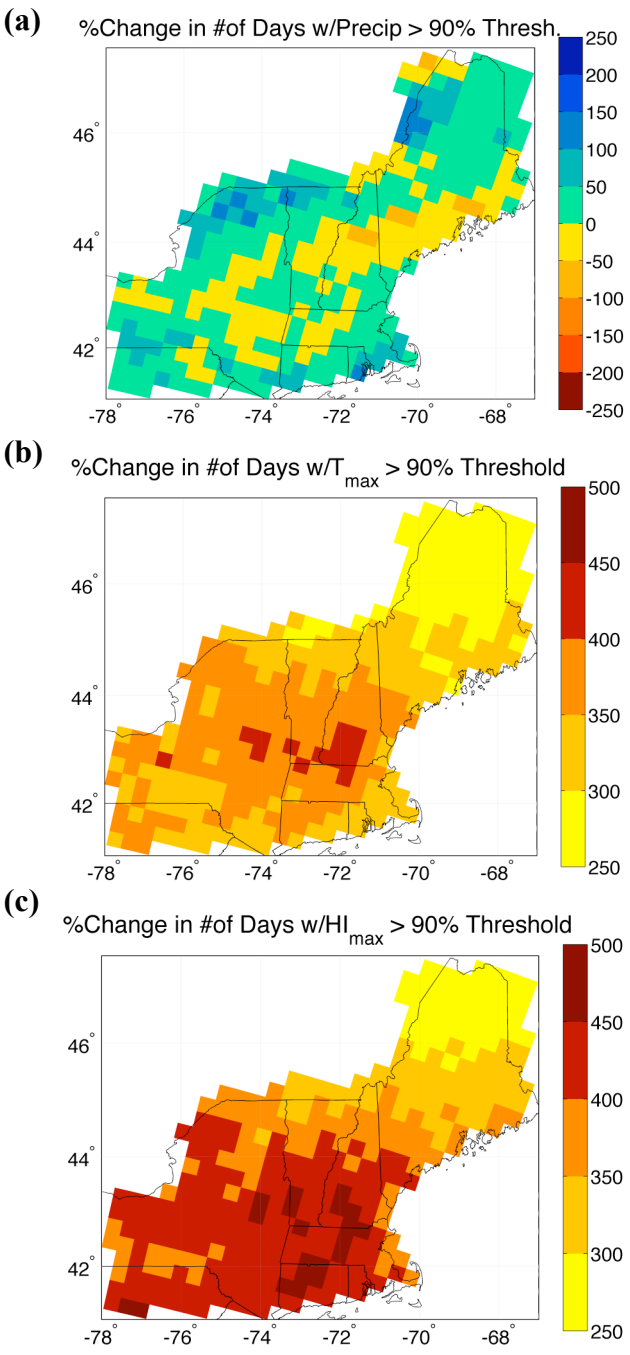

FIG.9 Percent change in number of days during 2090-99 experiencing daily (a) precipitation amounts, (b) maximum 2-meter air temperatures and (c) maximum Heat Index (HI) values greater than the 1990-99 10% exceedence threshold under the A1fi scenario.

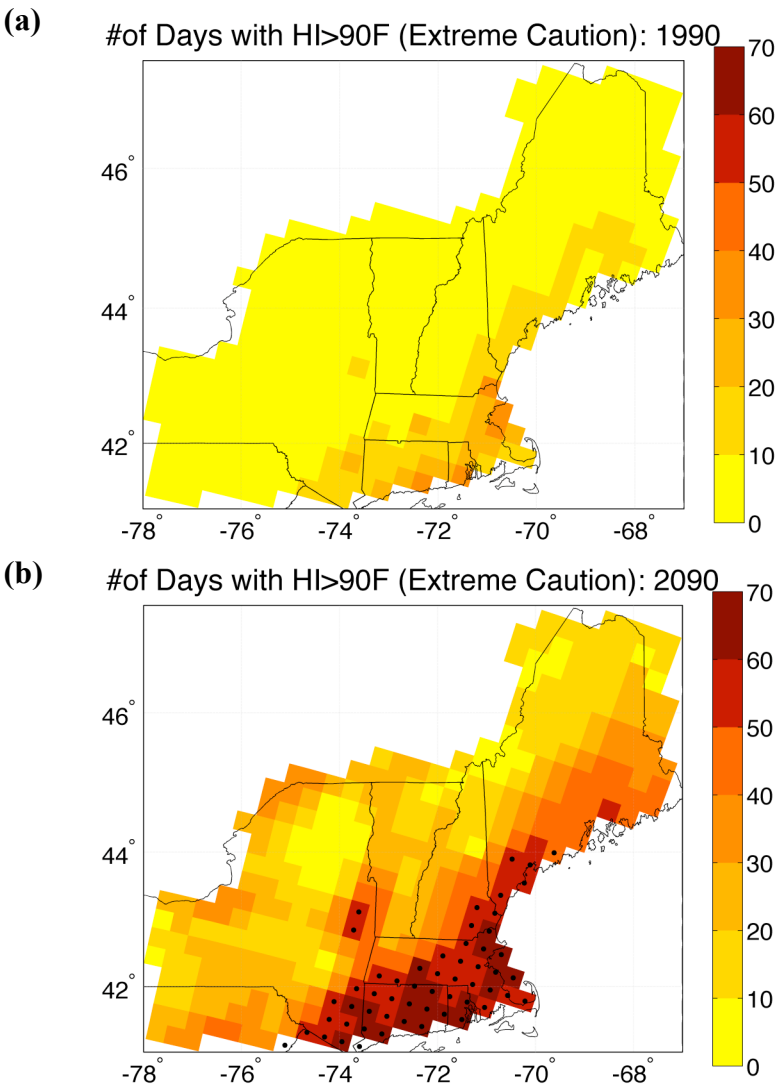

FIG.10 Number of days per 92-day summer season (June-August) in which the daily heat index (HI) maximum is above the National Weather Service "extreme caution" level (90°F) for (a) 1990-1999 and (b) 2090-2099. Regions with black dots are ones in which seasonal-mean daily HI maximum is above "extreme caution" level (90°F).

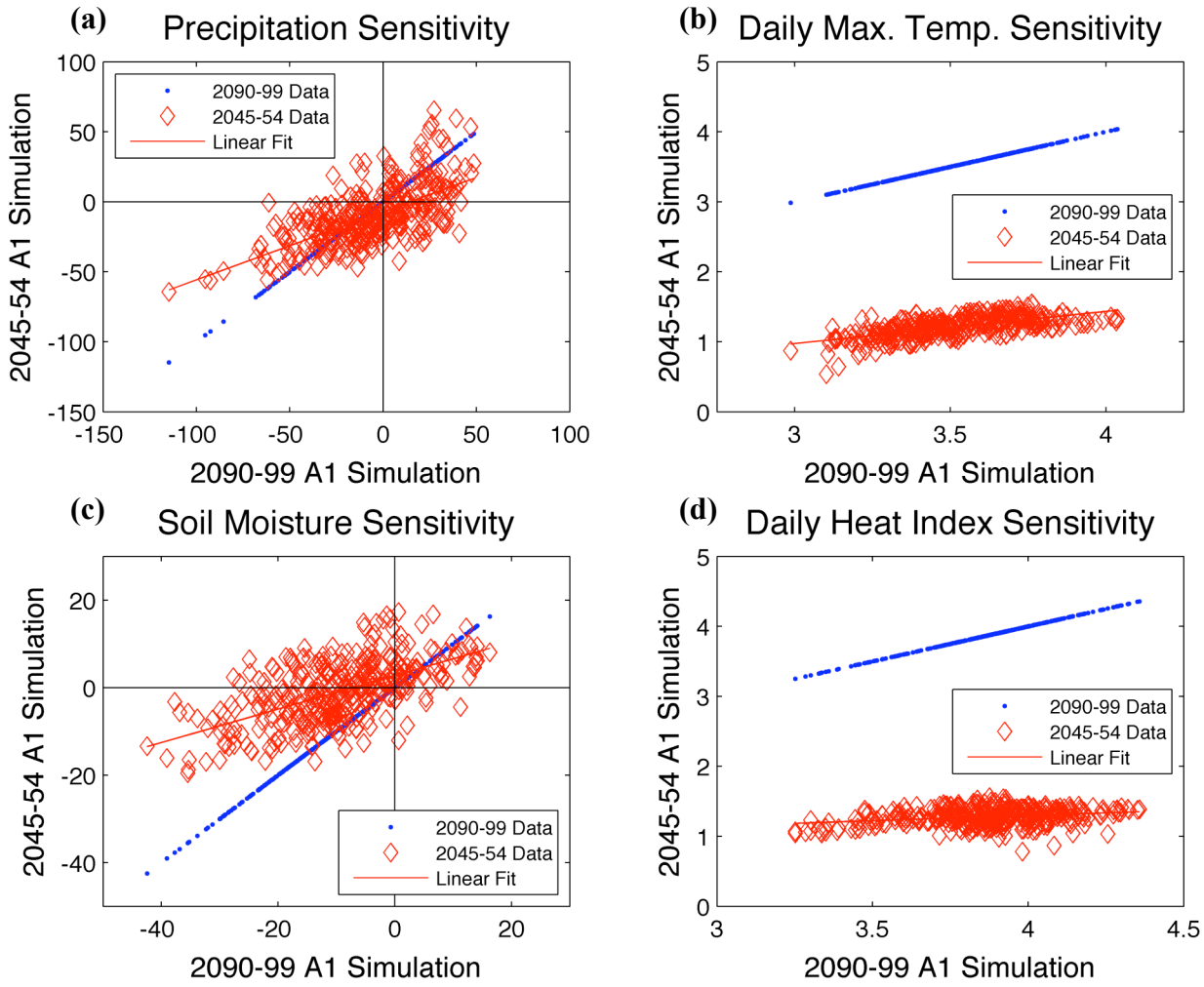

FIG.11 (a) Scatter plot of grid-point change in mean summertime precipitation (mm/season) between 1990-99 period and 2090-99 and 2045-54 periods, respectively, under the A1fi scenario. (blue) – 2090-99 precipitation anomalies plotted against themselves; (red) – 2045-54 precipitation anomalies plotted against the 2090-99 anomalies; (red line) – best-fit linear trend to the 2045-54 precipitation anomalies as plotted against the 2090-99 anomalies – see text for details. (b) same as (a) except for change in seasonal mean daily maximum temperatures (^{o}C). (c) same as (a) except for change in seasonal mean total soil moisture content (mm). (d) same as (a) except for change in seasonal mean daily maximum heat index (°C).